Proton exchange membrane fuel cell performance investigation considering internal heterogeneity of current density – A novel method study

Yu Jiang [1], Lei Huang [1], Xuexia Zhang [1,2,*], Lara Rasha[3], Dan J.L. Brett [3]

[1] *School of Electrical Engineering, Southwest Jiaotong University, Sichuan, Chengdu 611756, China*

[2] *National Rail Transportation Electrification and Automation Engineering Technology Research Center, Southwest Jiaotong University, Sichuan, Chengdu 611756, China*

[3] *Electrochemical Innovation Lab (EIL), Department of Chemical Engineering, University College London, London, WC1E 7JE, United Kingdom*

Abstract

The remaining useful lifetime (RUL) of proton exchange membrane fuel cell (PEMFC) has been influenced by the heterogeneous distribution. In this presented paper, a novel method considering the internal heterogeneity is proposed and investigated to manage the proton exchange membrane fuel cell (PEMFC) operation thus prolonging the remaining useful lifetime. This method including the mathematic steps of quantification, normalization, and coordinate transformation, converts the conventional power-current density curve into a novel power-heterogeneity curve. The electro-thermal mapping device is applied to measure the physical-field heterogeneity of a single cell during the polarization curve tests under different temperature conditions. This method is validated

* Corresponding author.
E-mail address: jy2425106569@my.swjtu.edu.cn (Y. Jiang); 15520668615@163.com (L. Huang); survival_zxx@sina.com (X. Zhang); lara.rasha.12@ucl.ac.uk (L. Rasha); d.brett@ucl.ac.uk (D. J. L. Brett).

by the results in the current region of 750 ~ 860 mA cm^{-2} of the polarization curves under temperature conditions of 50 °C and 60 °C. The novel method shows the effectiveness to make the fuel cell operate at a lower heterogeneity extent meanwhile a similar performance.

Keywords: proton exchange membrane fuel cell; heterogeneous distribution; quantification; normalization; coordinate transformation

1. Introduction

The increasing greenhouse effect and growing energy crisis have appealed to the rapid development and application of sustainable energy technologies. Recently, proton exchange membrane fuel cell (PEMFC) is a promising technology and application in the demand for renewable and sustainable energy [1–4]. Nevertheless, its commercialization process is restrained by the deficiencies of a short service lifespan [5,6] and expensive platiniferous materials [7,8]. At present, the platinum is still indispensable in membrane electrode assemblies (MEAs) for most PEMFCs, thus how to improve the operation strategy [9,10] to enhance the remaining useful lifetime (RUL) [11,12] and reduce usage costs [13] for technical PEMFCs is one of the primary concerns.

In recent, several studies [14–19] have reported that internal heterogeneity of physical-field distribution accelerates fuel cell degradation, leading to a decreased lifespan. Ferreira et al. [14] intercalated the decay model to a computational fluid dynamics model and found that oxygen distribution with poor disparity accelerates cell degradation. Moreover, the non-uniform degradation further leads to oxygen distribution unevenly and vice versa. At start-ups and shutdowns, it has been found that the transient heterogeneity of reactants [15–17] causes heterogeneous current distribution, further leading to severe material degradation in return. Dubau et al. [15] pointed out that MEA materials have significant heterogeneous degradation during accelerated stress tests. The heterogeneous distribution of current density leads to non-uniform thermal and water produce, of temperature results in local overheating even membrane drying, and of water content causes local flooding. These detrimental effects further increase the heterogeneity and even form a vicious circle conversely, as a result, reducing performance and shortening the lifespan of the PEMFC.

However, it is worth noting that, inside PEMFC, the heterogeneous distribution of the physical field is an inherent property caused by its size [20], flow-field design [21,22], transmission and reaction mechanism [23], and the material non-uniform distribution [24]. Moreover, the distributions are more heterogeneous in the scaled-up PEMFC for industrial purposes [15,20]. Over the years, the segmented cell [25] and print circuit board (PCB) [26,27] technologies are the primary means to measure and evaluate the physical field distribution inside PEMFC. Thus, how to reduce the heterogeneity of physical-field distribution [28], such as the local temperature, local current density and so forth [29–31], meanwhile maintaining efficient output performance [32] is of significance for improving PEMFC durability.

From the PEMFC perspective, a popular way in current to decrease the heterogeneity is the flow-field optimization and design [33,34]. Chen et al. [35] improved the parallel flow field to a stepped one, being experimental validation by polarization curve, the numerical results indicated that this new flow field not only reduces the areas of low oxygen concentration, low current density and flooding, but improves the homogeneity. A novel framework named metal foam flow-field was investigated in [22] and the numerical results indicated that it improves the reactant homogeneity inside the fuel cell. Bethapudi et al. [36] found that, according to the measured spatial distribution, the fractal flow-field PEMFC exhibits a more homogeneous distribution and assists to avoid the flooding effectively. Other types of flow-field design, such as lung-inspired [37], bio-inspired [38], and so on [39], enhance cell performance as well as reduce heterogeneity. Most studies focusing on PEMFC itself have obtained satisfactory results on continuously improving performance and reducing heterogeneity.

From the application perspective, it is to apply and test the PEMFC without changing its structural and geometric design. Hence, how to keep up the efficient output and maintain a more homogeneous distribution in the meanwhile is crucial to extending RUL. It has been indicated that heterogeneity is affected by operating conditions of temperature, pressure, current intensity, and the like [14,40,41]. Customarily, the PEMFCs avoid operating at low and high temperatures due to their weak performance and vulnerable component material in such cases [42]. Low temperatures lead to the PEMFC conductivity loss, sluggish reaction process [42], and suffering CO poisoning [43]. High temperatures result in the membrane losing mechanical stability [44] even encountering irreversible damage. For suitable temperatures, the strategy was reported to manage the operation in-depth, which is to select the better voltage or power at the identical current densities based on polarization curves [45]. Considering the effects of heterogeneity on RUL and the impact factors of heterogeneity, it is necessary to develop a strategy combining polarization curves to manage the PEMFC operation thus prolonging its RUL. However, little literature has reported the quantitative effects of heterogeneity on fuel cell RUL over the years.

The polarization curve is an effective way to evaluate the fuel cell overall performance [46,47], which is tested at a steady temperature and across the current range (generally from zero to limiting current) with the voltage recorded [41]. One of the principal applications of the polarization curve is to optimize the geometric structural parameters [32], operating conditions[45], and so forth, so that improving the PEMFC performance. As for industrial application scenarios [48] or simulated dynamic operation [49], whether the temperature is robust controlled at expected values is worth paying attention to due to the reactions continuously producing heat when the PEMFC delivers power to external

circuits [50–52]. The cell temperature increases as elapsed time lasts and the current intensity increases. Moreover, the temperature is difficult to be constrained at expected values in the case of dynamic load cycles. Therefore, Rasha et al. [41] reported a novel manner that the temperature is not get commanded during polarization curve tests to investigate the effects of the self-heating phenomenon on PEMFC performance.

This work is inspired by the studies on heterogeneous distribution affecting the PEMFC lifetime. This paper proposes a novel method to further manage the PEMFC operation based on the heterogeneous distribution. The principal contributions and the novelty are shown as follows. A numeric index is proposed to quantify the heterogeneous distribution of the local current density, which is measured by an electro-thermal mapping device[53]. This novel method consists of steps of quantification, normalization, and coordinate transformation. The conventional power versus current curve is transformed into the novel power versus heterogeneity curve using this method. The PEMFC can operate in the situation of the lower heterogeneity of current density meanwhile the similar performance in the specific current region. Thus, the fuel cell lifespan can be prolonged to some extent using this novel method.

The framework lays out as follows. Section 2 introduces the experimental setups and the testing procedures. Section 3 presents the quantification methodology, analysis of experimental results, and the novel plots of the method. Section 4 concludes this paper. In addition, the Appendix clarifies the detailed steps of normalization and coordinate transformation.

2. Experiment

2.1 Experimental setup

A single cell with an active area of 100 cm^2 is tested in this work [27]. For the MEA components, a 15 μm Gore M820.15 membrane (W. L. Gore & Associates, Inc.) is sandwiched by two 230 μm gas diffusion layers typed Freudenberg H23C9. The catalyst Pt loadings are 0.4 mg cm^{-2} (HyPlat Ltd) for both the anode and cathode sides. The serpentine-pattern channels are adopted for the flow field with the 1 mm channel width and depth as well as the 1 mm rib width. The exploded views of the cell are illustrated in Fig. 1a. In addition to the cell components, a mapping device is inserted into the cathode side, between the bipolar plate and the current collector.

The mapping device based on PCB technology is fabricated by S++ (S++ Simulation Service, Germany), which is applied to measure the electrical and thermal distribution of the fuel cell. The PCB-based mapping device covers a 100 cm^2 active area with an array of 14 × 14 shunt resistors with a 50.5 mm^2 current contact area for each one. This device also contains 7 × 7 uniformly distributed units to measure the local temperature. The schematic of the mapping device is shown in Fig. 1b, where the black bullets represent the shunt resistors to collect the current information and the red bullets represent temperature sampling points, respectively. The contact area between the current collector and the mapping device is presented by the square centered on each bullet. A Cartesian coordinate system is established and the gas flow orientations are displayed in Fig.1b to give a convenient explanation for the methodology in the following content. Here, the sampling points as labeled in Fig. 1b near the cathode inlet are appointed as the coordinate (1, 1) for electrical and thermal mapping plots, respectively.

2.2 Testing procedure

Fig. 1c shows the schematic of the testing system. The polarization curves of the cell are conducted using the experimental bench controlled by LabVIEW software (National

Instruments). The fuel and oxidant are supplied by BOC (London, UK) with the following properties: hydrogen (99.995% purity) and air (99.998% purity). The stoichiometric ratios are 1.5 and 3.0 for anode and cathode reactants, respectively. During the polarization curve tests, pure hydrogen with 30% RH (relative humidity) and the air is supplied along flow channels [41].

The cell temperature is not actively controlled once the start of the polarization curve tests for all the operating conditions. Three sets of experiments are conducted at various initial temperatures of 50 °C, 60 °C and 70 °C, respectively. It means that when the cell is preheated to the desired temperature, the heating subsystem is controlled to output a constant power to maintain the initial temperature. Moreover, heat dissipation is not taken through the experimental processes. In this way, when starting to test the fuel cell, a part of the generated heat is exchanged with the ambient and the rest is used for self-heating. Therefore, due to the self-heating, cell temperature continues to increase based on the initial temperature. The polarization curve is conducted with current density in 50 mA cm^{-2} step increment with each current density retained for 60 s. Tests are terminated when the total current rises to 130 A or the voltage declines to 0. During the testing process, the electrical and thermal mapping data, current intensity, and voltage response are recorded by the devices every 500 ms through the data acquisition system (DAQ).

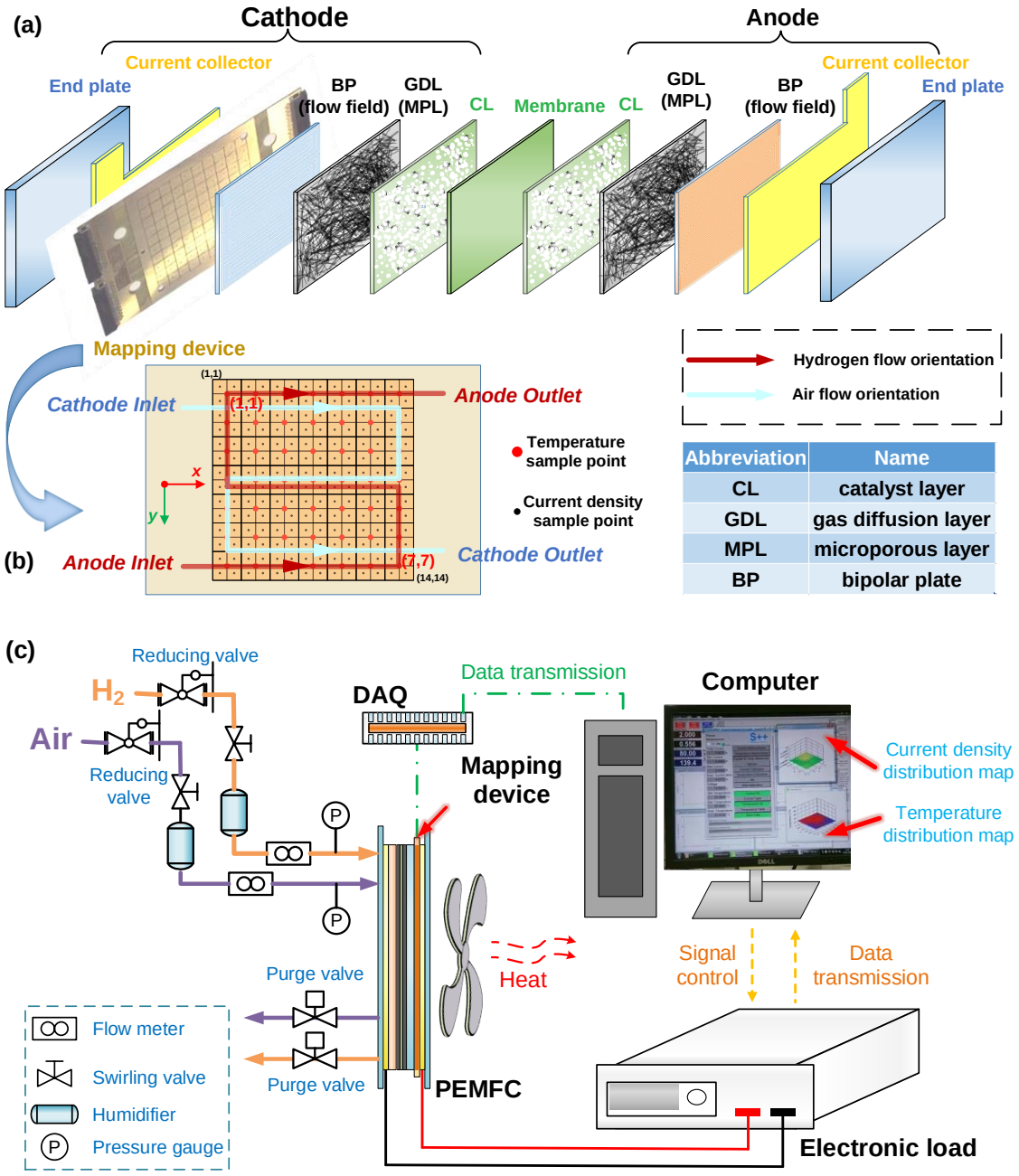

Fig. 1 (a) Exploded graph of the single fuel cell with a mapping device, (b) schematic diagram of the mapping device with the reactant flow orientations and a Cartesian coordinate system, and (c) schematic diagram of the testing system.

3. Results and discussion

3.1 Methodology – heterogeneity quantification

Heterogeneity quantification is proposed in this paper according to the mapping data to achieve the description and analysis of PEMFC performance from a novel perspective. In this case, the distributed current density and temperature are transformed into numerical matrices. Equations (1) and (2) represent the current and temperature distribution at each data record, respectively.

$$I(k)=\begin{bmatrix} i_{1,1} & \cdots & i_{1,14} \\ i_{2,1} & \cdots & i_{2,14} \\ \vdots & \ddots & \vdots \\ i_{14,1} & \cdots & i_{14,14} \end{bmatrix} \tag{1}$$

$$T(k)=\begin{bmatrix} t_{1,1} & \cdots & t_{1,7} \\ t_{2,1} & \cdots & t_{2,7} \\ \vdots & \ddots & \vdots \\ t_{7,1} & \cdots & t_{7,7} \end{bmatrix} \tag{2}$$

where *I*, *T* denotes the current and temperature profile, *k* is the sequence of the data record, and *i*, *t* indicates the local values of current density and temperature, respectively. Besides, the subscripts of each term in equations (1) and (2) indicate the position sampling points, which correspond to the mapping coordinates in Fig. 1b of current and temperature, respectively.

The standard deviation (*SD*), which is used to figure data distribution characteristics generally, is applied to quantify the physical field heterogeneity in this paper. The following contents show the steps of calculating the standard deviations. The data mean values are expressed as equations (3) and (4):

$$EI(k)=\frac{\sum_{m=1}^{14}\sum_{n=1}^{14} i_{m,n}}{14\times 14} \tag{3}$$

$$ET(k)=\frac{\sum_{j=1}^{7}\sum_{l=1}^{7}t_{j,l}}{7\times 7} \quad (4)$$

where *EI* and *ET* indicate the mean value of the current density and temperature for the *k*th mapping data, and subscripts *m*, *n*, *j*, *l* are the sequence number of matrix rows and columns corresponding to the position. Therefore, the *SD* values of current density and temperature can be expressed as equations (5) and (6):

$$SI(k)=\sqrt{\frac{\sum_{m=1}^{14}\sum_{n=1}^{14}\left(i_{m,n}-EI(k)\right)^2}{14\times 14-1}} \quad (5)$$

$$ST(k)=\sqrt{\frac{\sum_{j=1}^{7}\sum_{l=1}^{7}\left(i_{j,l}-ET(k)\right)^2}{7\times 7-1}} \quad (6)$$

where *SI* and *ST* express the standard deviation of the current density and temperature to quantify the heterogeneity for the *k*th mapping data in the time domain.

3.2 Polarization curves

The fuel cell performance under each condition is illustrated in Fig. 2, where the polarization curves and power versus current density curves are illustrated in Fig. 2a and 2b, the temperature varying curves are displayed in Fig. 2c as well. All the points in Fig. 2 are calculated by the mean values for each current intensity.

The PEMFC exhibits a preferable overall performance at 50 °C with greater limiting current density and maximal power, which is notable in Fig. 2a and 2b. Moreover, a reduction of limiting current density from 1314 mA cm^{-2} (50 °C) to 708 mA cm^{-2} (70 °C) can be observed in Fig. 2a with the initial temperature increases. Thereby, cell voltage drops and the maximal power declines according to the voltage-current relationships. The corresponding current density of peak power is closed to the concentration loss region

according to the power–current density plots in Fig. 2b and the peak power reduces by 47.3% from 57.7 W (50 °C) to 30.4 W (70 °C).

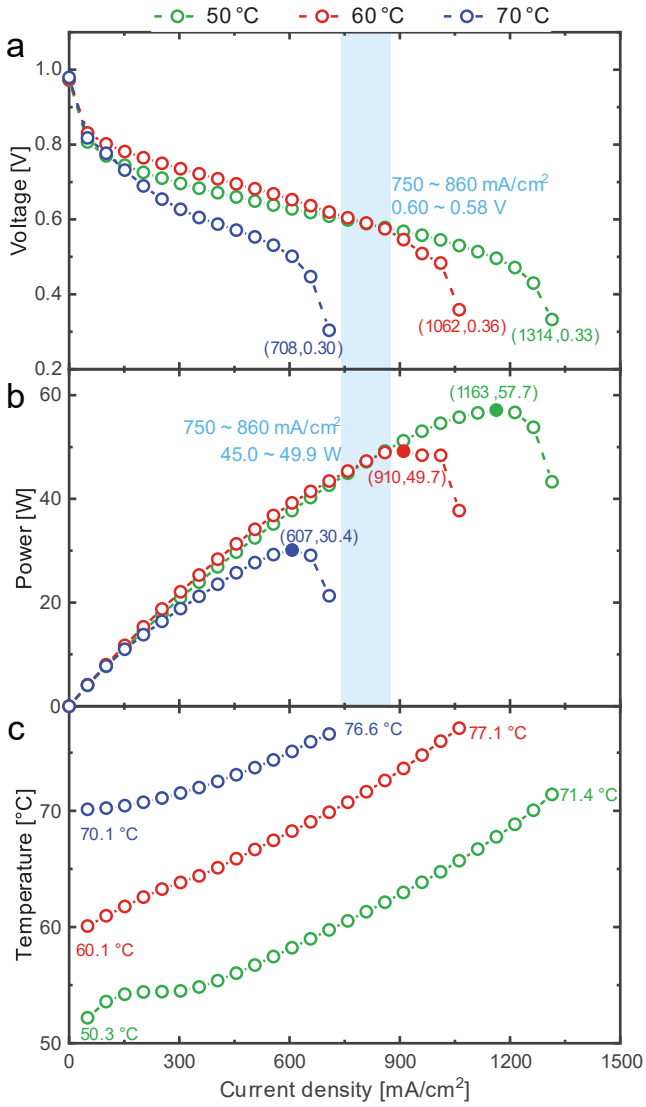

Fig. 2 The electrical parameters and temperature versus current density curves under the initial temperatures of 50 °C, 60 °C and 70 °C. (a) polarization curves; (b) power performance curves; and (c) temperature varying curves.

Previous studies [54,55] have demonstrated that limiting current density is reciprocally related to temperature and is greatly affected by water content inside the fuel cell, which has a decisive impact on oxygen diffusion in porous media layers, oxygen partial pressure in the catalyst layer, and air transport in channels. Plenty of liquid water is produced through the oxygen reduction reaction (ORR) when the fuel cell operates at high current

intensities, even though the elevated temperature has enhanced the saturated vapor pressure to reduce the water saturation. The liquid water, in the form of droplets, plugs and films, occupies the pores in porous media impeding the oxygen diffusion to reaction sites. Moreover, it attaches to channel walls, hindering air transport and even increasing the pressure drop. Therefore, the limiting current is affected and reduced according to the above mechanisms. Furthermore, the limiting current of the MEA component working at 70 °C or above is constrained by membrane dehydration as well.

Without active heat dissipation measures, as shown in Fig. 2c, the temperature rises 21.1 °C, 17 °C and 6.5 °C eventually, respectively, for three cases. Thus, it is significant that the thermal energy produced by the ORR heats the cell continuously with current increment and elapsed time. The primary reason for different temperature rises is that the fuel cell achieves a smaller limiting current in a higher initial temperature case. It is worth noting that, for the cases of 50 °C and 60 °C, despite the temperature continuously increasing up to more than 70 °C in the testing process, the current intensity can still be maintained and can even reach higher under this strict condition. In contrast with the former, the limiting current density only achieves 700 mA cm^{-2} when the initial temperature is 70 °C. Therefore, it can be regarded that the initial temperature or the initial humidity for the fuel cell has a greater impact on the performance and heterogeneity. The effects of initial conditions on fuel cell heterogeneity are discussed in depth in Section 3.3.

A current density region from 750 to 860 mA cm^{-2}, which is highlighted in light blue in Fig. 2a and 2b, contains similar voltage and power for the fuel cell. It can be noted from the polarization curve and power curve that, compared to the 60 °C case, it has, for the 50 °C case, a greater activation loss, less ohmic loss, and higher limiting current

density. Hence, the polarization and power curves of the two cases intersect and it can be observed the approximate performance in this highlighted region. Fuel cell performance in this current region is the core content of this paper and, in consideration of heterogeneity characteristics, it will be studied emphatically and in detail in the next sections.

The polarization performances are discussed under various initial temperatures in this part. The results indicate that temperature affects the limiting current and the performance. Temperature increase reduces the limiting current and a proper rise of the temperature can improve the output performance, yet too high the temperature could lead to local membrane dehydration. The initial temperature, under the same inlet conditions, is noteworthy that it can be one of the principal constraints for the performance and the limiting current density. A low initial temperature corresponds to a low liquid water saturation pressure, leading to more hydrated membrane regions and improving the fuel cell performance as a result.

3.3 Heterogeneity phenomena

The mapping results in Fig. 3 indicate that the current density is not uniformly distributed inside the fuel cell. The heterogeneity phenomena of mapping patterns and coordinate values vary with every record in the time domain. The authors note that, under the same total current, the time-series values of current density fluctuate near a constant value for each measurement point. Hence the contour images in Fig. 3 are composed of mean values at each condition. Different from the characteristics of current density images, the extreme values of temperature images are less than 2 °C in each data record, which is far below the operating temperature. Thus, the following contents mainly discuss the current density heterogeneity. Fig. 3a–3c compare the characteristics of current

density distribution under the same total current 50 A, and Fig. 3d and 3e are the statistics of the measured values under the total current intensity of 50 A and 80 A, respectively.

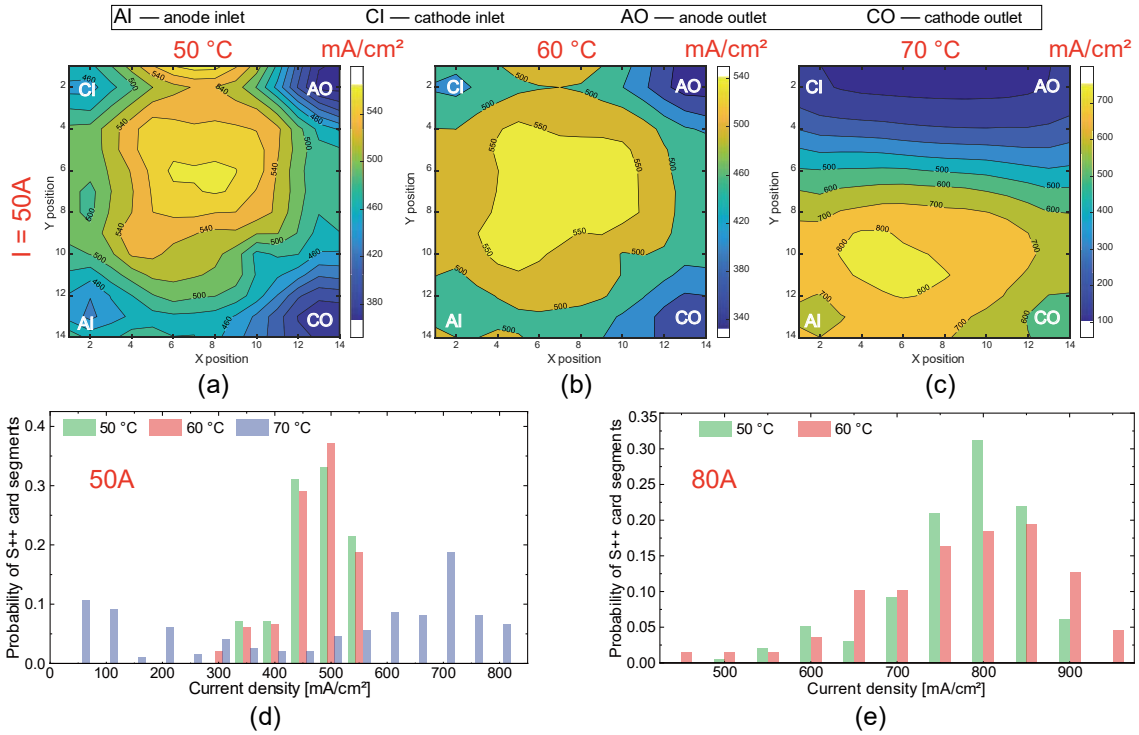

Fig. 3 The contour images of current density under the total current density for three conditions. (a) 50 °C; (b) 60 °C; and (c) 70 °C. The statistics of the measured data for each condition under the total current of (d) 50 A and (e) 80 A.

The distribution of current density, shown in Fig. 3a–3c, exhibits some characteristics that, for all three cases, the current density is concentrated in the MEA central region and is lower in the outlet regions. Another possibility for the outlet regions can be the deficient reactants. The reduction of reactant humidity can be derived from the increased initial temperature according to the relation of vapor saturation pressure versus temperature. The moist reactant meets a higher temperature and increases the vapor saturation, hence the reactant RH decreases due to the constant vapor pressure. Therefore, one explanation for the low current densities in local regions is that insufficient humidity causes a slower electrochemical reaction rate. With the reaction proceeding, the generated water at the cathode catalyst transfers to bipolar channels, and some back diffuses to the anode side

humidifying the membrane. Thus, the electrochemical reaction is accelerated in these regions inducing higher current densities. Moreover, comparing these contour images, the low current density regions and the extreme values get larger very slowly with temperature increase, resulting in a more heterogeneous distribution.

Fig. 3d and 3e, the data statistics of the contour images, intuitively reflect the distribution of measured current density in the probability form under the total current of 50 A and 80 A. It can be noted that, for the cases of 50 °C and 60 °C, most of the current densities concentrate in the interval of 450 ~ 550 mA cm^{-2}, and their extreme values are less than 250 mA cm^{-2}. However, compared with the former cases, it emerges a contrary trend of the data statistics for the case of 70 °C. The statistical features are that a large range from 50 to 800 mA cm^{-2}, current density distribution centralizing in near the extreme values, and only little data closed to 500 mA cm^{-2}. The local drying at the cathode inlet region causes a slow reaction rate and a current density; thus, large current densities are required in other regions to maintain the total current at 50 A. Similarly, it can be observed from the distribution characteristics at the current intensity of 80 A that the extreme value increases and the distribution probability of current density diverges to the sides.

The above discussion can be concluded that the increased temperature and current lead to a more non-uniform current density distribution. The gradients of current density increase among different regions, in this context, leading to a heterogeneous distribution in water content, pressure, and so forth. A more uneven degradation and structural changes of MEA components can be inferred due to the cell suffering non-uniform stress situation. The local materials degradation is accelerated under high temperature and

current intensity, resulting in reduced operation stability and remaining useful lifetime eventually.

3.4 Heterogeneity quantification of current density

The quantification results of the mapping data are discussed in this section, where Fig. 4 shows the *SD* values in the time domain containing the current intensity in the subplot, and Fig. 5 illustrates the *SD* values versus current density with error bars. The relative error calculated by extremums, which is superimposed to each mean value and the mean value under each current density are applied to reflect the oscillating extent in the time domain.

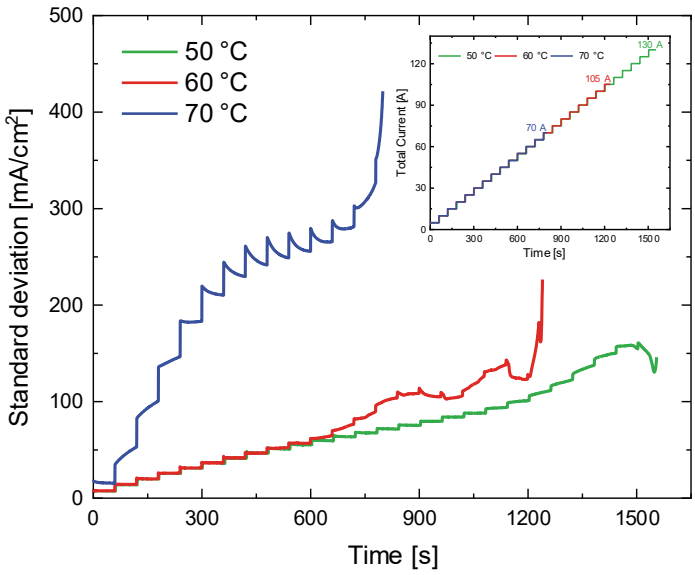

Fig. 4 The varying trend of standard deviation values versus current density in the time domain, with the total current intensity in the subplot.

The varying trend of *SD* values in time domain is similar to the current profile with step changes. It can be noted from Fig. 4 that the increases in temperature not only reduce fuel cell limiting current, but also cause an unstable *SD* value in the time domain. In addition, The *SD* values cannot maintain a constant value and increase with elapsed time when the fuel cell provides a large current to the external circuit. Even when the current increases to the limiting current, the *SD* values rise sharply in a very short time. From the

temperature perspective, the *SD* value for the 70 °C case increases with current intensity and the elapsed time from 0 to 300 s, while it descends gradually with time duration when the current is stable in the time interval of 300 to 750 s.

It can be described using the membrane wetness for the abovementioned phenomenon that the ORR process produces a small amount of water when the PEMFC outputs small currents. The generated water raises with the current density increment and elapsed time, inducing the reverse osmosis of water molecules to humidify the anode side of the membrane. Thus, the current density distribution becomes stable under the improved hydration environment slowly. The *SD* values for 50 °C and 60 °C cases show the similarity in values and trends before the current intensity up to 50 A (~ 600 ms). With the elapsed time and current increment, the inconsistency between the two curves becomes clear since 50 A. On the other hand, the *SD* values are stable for 50 °C (< 95 A) and 60 °C (< 50 A), whereafter the curves are changing with elapsed time after the current increase.

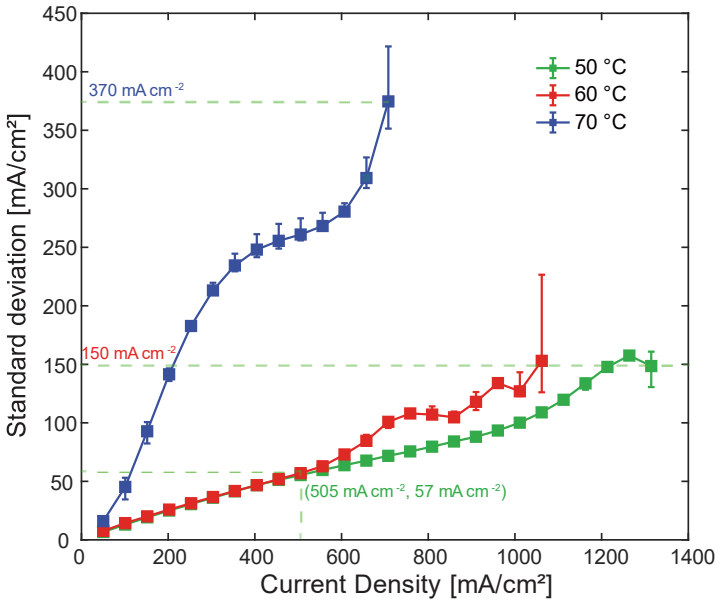

Fig. 5 The *SD* values of current density under the cases of 50 °C, 60 °C and 70 °C in the current domain with error bars.

Fig. 5 displays the *SD* values with error bars in each case in the current domain. It can be noted that the errors are more significant when near the limiting current density. The *SD* values increase from a small value at 50 mA cm^{-2} to the maximum around the limiting current. Where the *SD* maximum is about 150~160 mA cm^{-2} for both 50 °C and 60 °C, and about 370 mA cm^{-2} for 70 °C. For the curves of suitable temperatures, it can be divided into two parts: the first part is that *SD* values increase reposefully in linearity form until 500 mA cm^{-2} for 60 °C and 1000 mA cm^{-2} for 50 °C, where the values are almost the same in the region of 50 ~ 500 mA cm^{-2} for both temperature cases; another part is the non-linear part of the increase with current increment. On the other hand, the plot of the case at 70 °C shows the ascending trend of rapid–steady–rapid corresponding current ranges of 0 ~ 300 mA cm^{-2}, 300 ~ 500 mA cm^{-2} and 500 mA cm^{-2} to the limiting current density. The quantification results demonstrate that the current increase leads to a more heterogeneous distribution inside the fuel cell. Furthermore, not only the limiting current density but the heterogeneity of current density is influenced by increased temperature. When the fuel cell operates at the 70 °C case, the *SD* values increase rapidly with the total current increment due to the local overheating causing membrane drying and even leading to heterogeneous transport of protons across the membrane plane. Another rapid increase trend exists at limiting current density, where the oxygen pressure in the cathode triple-phase boundary approaches zero and the current cannot be maintained continuously. Thereby the heterogeneity of current density is increased in this case.

To sum up, the results indicate that the internal heterogeneity is affected by coupling parameters. It is further demonstrated from the analysis of this section that the increases in temperature and current intensity, especially the initial cell temperature increment induce a more heterogeneous current density distribution. Moreover, the increase of

current density non-uniformity at the fuel cell operating at high temperatures is primarily caused by the small current densities in the drying regions. Such regions need higher current densities in other regions to get a match to hold the fuel cell current. The results of the heterogeneity quantification in the time domain more intuitively exhibit the dynamic changes with current intensity and elapsed time under different conditions.

3.5 Power performance considering current density heterogeneity

In consideration of the practical industrial systems, the load power is generally supplied by fuel cell stacks with temperature control to avoid overheating. Section 3.2 has discussed the performance in Fig. 2 and it can be noted that the fuel cell at 60 °C case performs better than that at 50 °C case before the current density increases to 800 mA cm^{-2}. Conventionally, the fuel cell is usually operated at higher temperatures and current intensities to enhance the power delivery. However, the results in Section 3.4 demonstrate that current density distribution is affected by both temperatures and current intensities, which results in the non-uniform degradation of MEA. Therefore, it is necessary to take into the heterogeneous characteristics of physical-field distribution account while ensuring fuel cell efficient performance.

There is a current region of 750 to 860 mA cm^{-2}, as shown in Fig. 2 and the analysis in Section 3.2, that the fuel cell has a similar performance at the same current for different temperature conditions. The fuel cell can be operated at either temperature case due to the conventional method placing importance on the performance. Just as the lifetime is a crucial issue for the commercial fuel cells, the temperature influences the internal heterogeneity, which affects the fuel cell lifetime in turn. It is of certain deficiency for the conventional method to guide the fuel cell operation in the aforesaid current region. Hence, a novel method concerning the fuel cell performance and lifetime are essential to

be proposed to manage the fuel cell operation in-depth, prolonging the remaining useful lifetime. Hereinto, the fuel cell lifetime can be characterized by a related index, i.e. heterogeneity degree in this paper.

In this section, a novel method is proposed and clarified by taking into the quantification results of physical-field heterogeneity as an index of the state of health (SOH). In this case, the power performance is a multivariate function as expressed in equation (7):

$$P = f\left(V, I, \mathrm{H}\right) \tag{7}$$

where P denotes the output power, V and I are the cell voltage and total current, and H represents the heterogeneity index. The following contents are used to state the power versus heterogeneity relationship in detail. Fig. 6 illustrates the power plots at 50 °C and 60 °C as well as their difference, which is calculated by the values of the latter subtracting the corresponding values of the former. Fig. 7 displays the quantification values of current density heterogeneity, where the *SD* values are processed by the normalization method shown as expression (8):

$$HI\left(k\right) = \frac{SI\left(k\right) - SI_{\min}}{SI_{\max} - SI_{\min}} \tag{8}$$

where $HI(k)$ with the value range [0, 1] is the normalized results of current density for the kth data and the subscripts max and min are maximum and minimum during the test.

It can be noted in Fig. 6 that the power difference shows a ascend–descend varying trend with current increment, where the maximum is 1.68 W at the current density of 505 mA cm^{-2} and corresponding powers are 34.48 W for 60 °C case and 32.80 W for 50 °C case, respectively. Since 505 mA cm^{-2}, the power difference declines gradually to 0.13 W where the power performance approximates 47.80 W for both conditions at 809 mA cm^{-}

^{2} and drops rapidly when the current density exceeds 850 mA cm^{-2}. Without considering the heterogeneity, the conventional operating strategy is generally to optimize the fuel cell to have a better performance at the same current. Therefore, as shown in Fig. 6, the fuel cell can be continuously operated at 60 °C under the corresponding power demands. As for large power demand, it should be operated at 50 °C case due to its extended limiting current density and higher peak power performance.

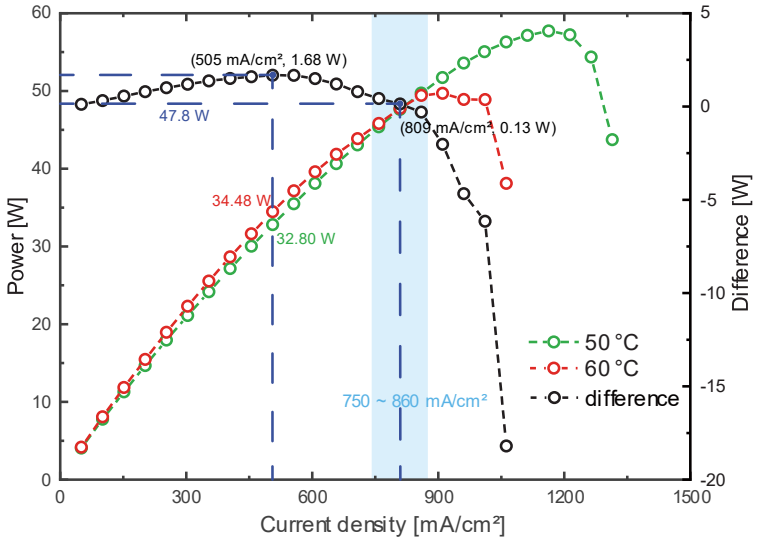

Fig. 6 Power performance as well as its difference in the current domain for the cases of 50 °C and 60 °C.

On condition that the heterogeneity is considered, as shown in Fig. 7, the PEMFC can be operated in the current region 0 ~ 505 mA cm^{-2} under 60 °C case due to the higher power performance and the similar heterogeneity. At the current density of 809 mA cm^{-2} and the approximate performance, the normalized quantification value of current density is 0.68 for the 60 °C case, which is larger than the value of 0.48 for the 50 °C case. In the region of 505 ~ 809 mA cm^{-2}, it should be noted that the power difference declines while the heterogeneity difference increases with the current increment. It is complicated for the fuel cell operating in this region to balance the performance and heterogeneity.

Therefore, an operating strategy that comprehensively considers performance and heterogeneity is essential for this region.

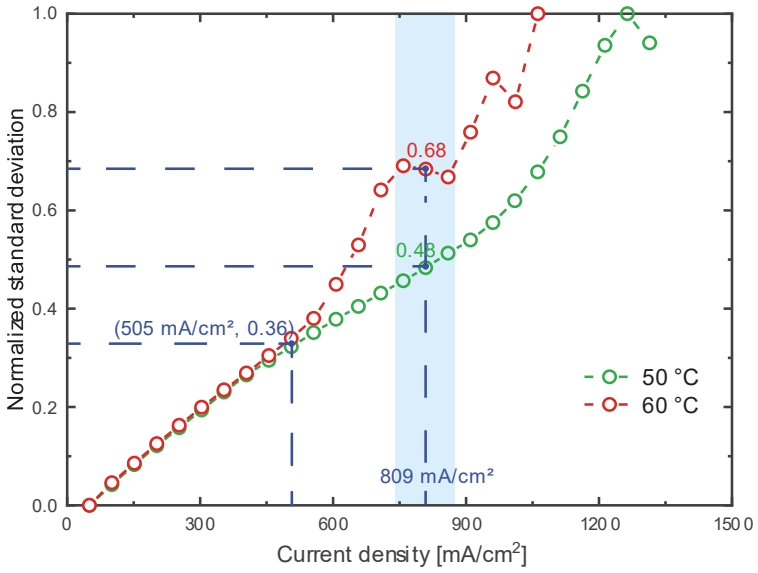

Fig. 7 The normalized heterogeneity quantification of current density distribution for 50 °C and 60 °C.

It is demonstrated in Fig. 6 and Fig. 7 that the cell power, in addition to total current and voltage, is related to the heterogeneity of local current density. Moreover, the cell power versus heterogeneity plots as well as their fitting curves is illustrated in Fig. 8 to describe the relationships in detail. For convenience, the normalized results of heterogeneity are adopted to investigate the varying trend of power. MATLAB Curve Fitting Toolbox® is applied to fit the points by custom equations, and the expression form and feasibility are evaluated at the temperatures of 50 °C and 60 °C.

In Fig. 8, the *y*-axis represents the power performance and the *x*-axis shows the normalized value *HI* for the current density. The shape of the curves is similar to the power versus current curves in Fig. 2, which indicates that the fuel cell performs similarly at lower *HI* values under different temperatures. When the *HI* values exceed 0.5, the PEMFC performs much better and has a small heterogeneity under the same power demand for the 50 °C case.

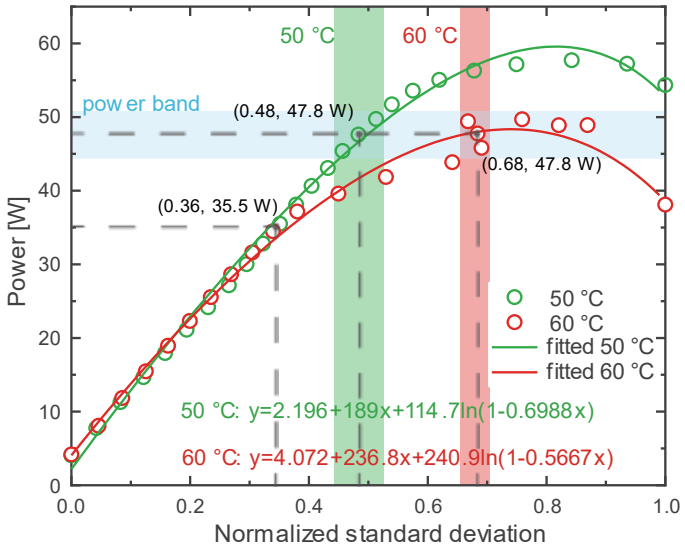

Fig. 8 The plots of power performance versus the heterogeneity of current density, fitting curves, and approximate expressions, for the cases of 50 °C and 60 °C. The shaded rectangular regions of the overlapped color bands represent the similar performance in the polarization curve and power curve in Fig. 6.

On the other hand, the highlighted rectangular regions in Fig. 8 are used to emphasize the distinction between this novel investigation and the conventional strategy. There are two vertical bands and one horizontal band, which corresponds to the *HI* values of 50 °C and 60 °C, and the power performance, respectively. The highlighted rectangles are the crossed region of the horizontal band and two vertical bands. Furthermore, the points inside are that their y-axis values correspond to the power performance in Fig. 6, and *x*-axis values can be correlated to the current density in Fig. 7. Thus, it can be derived that the points in the highlighted rectangles have the approximate power performance and current densities. As a result, despite the similar performances in the current region, the fuel cell is better to operate at the 50 °C case due to the much lower heterogeneity extent.

Therefore, it is better, according to Fig. 8 for this fuel cell, to be operated at 50 °C case when the power demands are over 35.5 W as well as the heterogeneity of current density beyond 0.36. Moreover, the fitting expressions suggest that the functional relationship expressed by equation (9) is suitable for both curves.

$$P(HI) = P_0 + A \times HI + B \ln(1 - C \times HI) \quad (9)$$

where P_0 denotes the power value at HI = 0 (calculated by equation (8)), A, B and C are the coefficients fitted by curves. The fitted curves shown in Fig. 8 represent a good fitting characteristic for both cases.

A novel investigation perspective considering heterogeneity is proposed in this section, which can be used to enhance the lifespan while maintaining efficient power performance. The conventional strategy emphasizes performance while this novel one takes care of the lifetime simultaneously. For the similar performance region of 750 to 860 mA cm^{-2}, this novel methodology exhibits its superiority and can well manage the fuel cell to operate at a lower heterogeneity. Thus, this novel method is beneficial for the remaining useful lifetime of fuel cells. In addition, the fitting curves with their expressions on experimental results are analyzed as well, which is promising in control engineering to extend the lifespan. This study in consideration of heterogeneity can be adopted during the fuel cell operation.

4. Conclusion

This paper proposes a novel method considering heterogeneous current density inside PEMFC to manage the operation as well as prolong the lifetime. The heterogeneous distribution is simultaneously measured by a PCB-based electro-thermal mapping device in the process of polarization curve tests. The feasibility and effectiveness of this method are validated by the current density region (750 ~ 860 mA cm^{-2}) of the intersectant polarization curves under temperature conditions of 50 °C and 60 °C. The results and discussions on figures and data conclude below:

1) The quantification results, i.e. the standard deviation in this paper, can be used to transform the distribution contour into numeric data and assist to establish the relations between power performance and heterogeneity.

2) The increasing temperature and current density lead to a more heterogeneous distribution; moreover, the initial temperature has a significant effect on the current density distribution.

3) This method consisting of the mathematic steps of quantification, normalization, and coordinate transformation, provides a novel perspective of converting the power-current curve into power-heterogeneity curve to manage the fuel cell operation thus to improve its durability.

4) In a specific region, the PEMFC operates a similar output performance meanwhile a lower heterogeneity of current density in the guidance of this method.

The novelty of this paper is to provide a thought based on heterogeneity to improve the fuel cell durability due to the quantitative effects of heterogeneity on fuel cell degradation that haven't been investigated. This paper provides a new approach between qualitative and quantitative studies of the effects of heterogeneity on lifetime to further manage the fuel cell operations. In future work, we will study the quantitative effects of heterogeneity on fuel cell lifetime, investigate the corresponding functional relationship, and study the current distribution under real PEMFC situations to extend the generality of this method.

Acknowledgments

This work was supported by the National Natural Science Foundation (51607149), Department of Science and Technology of Sichuan Province (2019YJ0236), key research

and development plans (major science and technology projects) of Sichuan province (22ZDYF3375).

Appendix – Method steps and example

A1. Steps

Convert the measured results of the distributed data into a matrix, which is expressed as:

$$I(k)=\begin{bmatrix} i_{1,1} & \cdots & i_{1,14} \\ i_{2,1} & \cdots & i_{2,14} \\ \vdots & \ddots & \vdots \\ i_{14,1} & \cdots & i_{14,14} \end{bmatrix} \tag{A.1}$$

Calculate the mean value of the measured data.

$$EI(k)=\frac{\sum_{m=1}^{14}\sum_{n=1}^{14} i_{m,n}}{14\times 14} \tag{A.2}$$

Afterward, calculate the standard deviation to quantify the distribution characteristic.

$$SI(k)=\sqrt{\frac{\sum_{m=1}^{14}\sum_{n=1}^{14}\left(i_{m,n}-EI(k)\right)^2}{14\times 14-1}} \tag{A.3}$$

Normalization process to limit the range from zero to one.

$$HI(k)=\frac{SI(k)-SI_{\min}}{SI_{\max}-SI_{\min}} \tag{A.4}$$

Customarily, the quantification result is approximate to zero when the test begins from a small current intensity. Hence, the $SI_{\min}$ can be ignored and the equation (A.4) simplified as:

$$HI(k)=\frac{SI(k)}{SI_{\max}} \tag{A.5}$$

$$P = f\left(V, I, \mathrm{H}\right) \tag{A.6}$$

For different temperature cases of T_1 and T_2 ($T_2 > T_1$), the output power versus heterogeneity quantification can be expressed as:

$$\begin{aligned} P_1 &= f\left(\mathrm{H}_1\right) \\ P_2 &= f\left(\mathrm{H}_2\right) \end{aligned} \tag{A.7}$$

where H denotes the quantification results *HI* in equation (A.4). In this paper, the fitted curve has the expression form as shown in equation (A.7):

$$P\left(HI\right) = P_0 + A \times HI + B\ln\left(1 - C \times HI\right) \tag{A.8}$$

As the maximal values of heterogeneity quantification are not the same under different temperature cases. Generally, during the overall polarization curve testing, the fuel cell exhibits a more heterogeneous distribution under higher temperature conditions.

Thus, suppose

$$SI_{1,\max} = \alpha SI_{2,\max} \tag{A.9}$$

where $0 < \alpha < 1$. Substitute equation (A.9) into equation (A.5), that is

$$HI_1 = \frac{1}{\alpha} HI_2 \tag{A.10}$$

Equation (A.10) is a stretching transformation for the *x*-axis in the Cartesian coordinate system. Therefore, the *x*-axis range is still the normalization value "1" and both cases have the same real value.

In this case, equation (A.7) can be transformed into

$$\begin{aligned} P_1 &= f\left(\mathrm{H}/\alpha\right) \\ P_2 &= f\left(\mathrm{H}\right) \end{aligned} \tag{A.11}$$

In this way, the two plots have the same output power corresponding to the same real value for the heterogeneity quantification results.

Substitute equation (A.11) into equation (A.8), the expressions for two cases are:

$$\begin{aligned} P_1(\mathrm{H}) &= P_0^1 + A_1 \times (\mathrm{H}/\alpha) + B_1 \ln\left[1 - C_2 \times (\mathrm{H}/\alpha)\right] \\ P_2(\mathrm{H}) &= P_0^2 + A_2 \times \mathrm{H} + B_2 \ln(1 - C_2 \times \mathrm{H}) \end{aligned} \tag{A.12}$$

A2. Example

For your convenience, the authors give an example here. Hereinto, the assumptions are drawn as follows.

i. The polarization curves interact and the authors defined a crossed region;

ii. The polarization curve is tested from a small current to the limiting current;

iii. The maximum standard deviation *SI*s have the relationship: $SI_{1,\,max}=0.85SI_{2,\,max}$.

It is supposed two cases T_1 and T_2 in Fig. A1 and the curve is plotted by the expression (A8) with different assumed parameters.

Thereinto, we have assumed a power band that is a similar performance region in their polarization curves. According to the analysis in the main text, the points in squares S1 and S2 correspond to similar points in their polarization plots. It can be noted that the corresponding *x*-axis ranges of range T1 and range T2 are close to each other before the coordinate stretching transformation.

Due to the maximum values, for the heterogeneity quantification, being unequal under two temperature cases T_1 and T_2, the stretching transformation is applied according to assumption iii and the equations (A9), (A5), and (A10) to make the coordinate of the two cases have the same conception. The power versus heterogeneity plot being coordinate transformed is illustrated in Fig. A2.

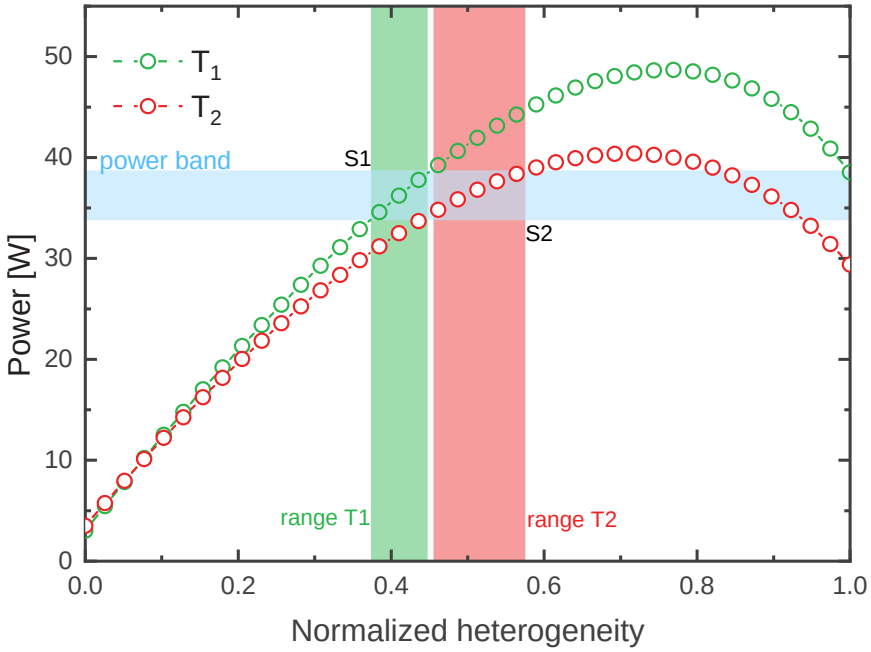

Fig. A1 The power versus heterogeneity curve under different temperature conditions.

It can be noted that, after transformation, the power curve of case T_1 and the square S1' has a left shift while another curve of case T_2 maintains. Comparing the two figures, the results indicate that the corresponding color bands of two crossed squares become more distinctive in Fig. S2. Thus, the fuel cell has a better homogeneity at case T_1 when it operates in a similar region, where the output power is approximate under identical current intensities.

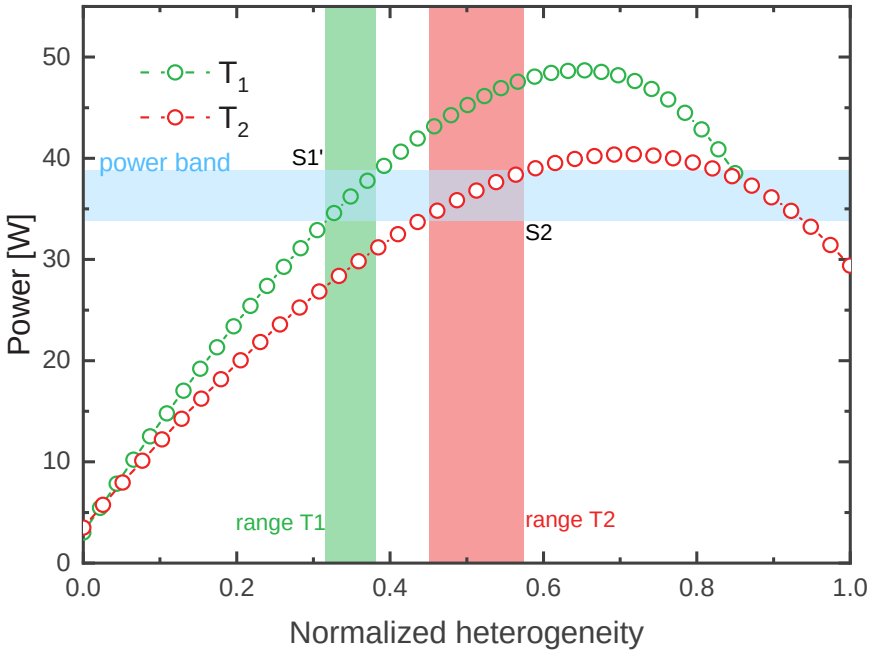

Fig. A2 The power versus heterogeneity curve after coordinate transformation under different temperature conditions.

It is customarily for PEMFC to have a similar performance under different conditions. From the conventional manner, the PEMFC can operate at either condition to output equal power intensities. However, the remaining useful lifetime issue has become one principal constraint with the fuel cell scale-up and commercialization. Moreover, there have been studies that reported that the physical-field heterogeneity inside MEA affects the PEMFC remaining useful lifetime. Hence, it is of importance and necessity to pay attention to the output performance meanwhile internal heterogeneity during operation. Under the guidance of this innovative method, the fuel cell can operate efficiently meanwhile have a better internal homogeneity. Thus, the fuel cells have a longer remaining useful lifetime ultimately under the suggestion of this method.

In the proposing process, the method only carried out data conversion and coordinate transformation in mathematics, while did not change the actual conditions or restrict the fuel cell operation. Thus, this proposed method is universal and feasible for guiding the fuel cell operation.

References

[1] Trogadas P, Cho JIS, Kapil N, Rasha L, Corredera A, Brett DJL, et al. Effect of extended short-circuiting in proton exchange membrane fuel cells. Sustain Energy Fuels 2020;4:5739–46. https://doi.org/10.1039/d0se00943a.

[2] Mittal VO, Kunz HR, Fenton JM. Membrane Degradation Mechanisms in PEMFCs. J Electrochem Soc 2007;154:B652–6. https://doi.org/10.1149/1.2734869.

[3] Jouin M, Gouriveau R, Hissel D, Péra MC, Zerhouni N. Prognostics and Health Management of PEMFC - State of the art and remaining challenges. Int J Hydrogen Energy 2013;38:15307–17. https://doi.org/10.1016/j.ijhydene.2013.09.051.

[4] Wu Z, Zhu P, Yao J, Tan P, Xu H, Chen B, et al. Thermo-economic modeling and analysis of an NG-fueled SOFC-WGS-TSA-PEMFC hybrid energy conversion system for stationary electricity power generation. Energy 2020;192:116613. https://doi.org/10.1016/j.energy.2019.116613.

[5] Chen H, Song Z, Zhao X, Zhang T, Pei P, Liang C. A review of durability test protocols of the proton exchange membrane fuel cells for vehicle. Appl Energy 2018;224:289–99. https://doi.org/10.1016/j.apenergy.2018.04.050.

[6] Zhang X, Yu Z, Chen W. Life Prediction Based on D-S ELM for PEMFC. Energies 2019;12:3752. https://doi.org/10.3390/en12193752.

[7] Gwak G, Lee J, Ghasemi M, Choi J, Lee SW, Jang SS, et al. Analyzing oxygen transport resistance and Pt particle growth effect in the cathode catalyst layer of polymer electrolyte fuel cells. Int J Hydrogen Energy 2020;45:13414–27. https://doi.org/10.1016/j.ijhydene.2020.03.080.

[8] Reshetenko T, Laue V, Krewer U, Artyushkova K. Study of degradation and spatial performance of low Pt-loaded proton exchange membrane fuel cells under exposure to sulfur dioxide in an oxidant stream. J Power Sources 2020;458:228032. https://doi.org/10.1016/j.jpowsour.2020.228032.

[9] Xu L, Li J, Ouyang M, Hua J, Yang G. Multi-mode control strategy for fuel cell electric vehicles regarding fuel economy and durability. Int J Hydrogen Energy 2014;39:2374–89. https://doi.org/10.1016/j.ijhydene.2013.11.133.

[10] Wu X, Xu L, Wang J, Yang D, Li F, Li X. A prognostic-based dynamic optimization strategy for a degraded solid oxide fuel cell. Sustain Energy Technol Assessments 2020;39:100682. https://doi.org/10.1016/j.seta.2020.100682.

[11] Jouin M, Bressel M, Morando S, Gouriveau R, Hissel D, Péra M-C, et al. Estimating the end-of-life of PEM fuel cells: Guidelines and metrics. Appl Energy 2016;177:87–97. https://doi.org/10.1016/j.apenergy.2016.05.076.

[12] Hua Z, Zheng Z, Pahon E, Péra M-C, Gao F. Remaining useful life prediction of PEMFC systems under dynamic operating conditions. Energy Convers Manag 2021;231:113825. https://doi.org/10.1016/j.enconman.2021.113825.

[13] Zhao J, Li X. A review of polymer electrolyte membrane fuel cell durability for vehicular applications: Degradation modes and experimental techniques. Energy Convers Manag 2019;199:112022. https://doi.org/10.1016/j.enconman.2019.112022.

[14] Ferreira RB, Falcão DS, Pinto AMFR. Simulation of membrane chemical degradation in a proton exchange membrane fuel cell by computational fluid dynamics. Int J Hydrogen Energy 2021;46:1106–20. https://doi.org/10.1016/j.ijhydene.2020.09.179.

[15] Dubau L, Castanheira L, Maillard F, Chatenet M, Lottin O, Maranzana G, et al. A review of PEM fuel cell durability: Materials degradation, local heterogeneities of aging and possible mitigation strategies. Wiley Interdiscip Rev Energy Environ 2014;3:540–60. https://doi.org/10.1002/wene.113.

[16] Durst J, Lamibrac A, Charlot F, Dillet J, Castanheira LF, Maranzana G, et al. Degradation heterogeneities induced by repetitive start/stop events in proton exchange membrane fuel cell: Inlet vs. outlet and channel vs. land. Appl Catal B Environ 2013;138–139:416–26. https://doi.org/10.1016/j.apcatb.2013.03.021.

[17] Schneider IA, von Dahlen S. Start-Stop Phenomena in Channel and Land Areas of a Polymer Electrolyte Fuel Cell. Electrochem Solid-State Lett 2011;14:B30. https://doi.org/10.1149/1.3518520.

[18] Chandesris M, Guetaz L, Schott P, Scohy M, Escribano S. Investigation of Degradation Heterogeneities in PEMFC Stack Aged under Reformate Coupling In Situ Diagnosis, Post-Mortem Ex Situ Analyses and Multi-Physic Simulations. J Electrochem Soc 2018;165:F3290–306. https://doi.org/10.1149/2.0321806jes.

[19] Hu Z, Xu L, Li J, Gan Q, Xu X, Song Z, et al. A novel diagnostic methodology for fuel cell stack health: Performance, consistency and uniformity. Energy Convers Manag 2019;185:611–21. https://doi.org/10.1016/j.enconman.2019.02.031.

[20] Peng L, Shao H, Qiu D, Yi P, Lai X. Investigation of the non-uniform distribution of current density in commercial-size proton exchange membrane fuel cells. J Power Sources 2020;453:227836. https://doi.org/10.1016/j.jpowsour.2020.227836.

[21] Azarafza A, Ismail MS, Rezakazemi M, Pourkashanian M. Comparative study of conventional and unconventional designs of cathode flow fields in PEM fuel cell. Renew Sustain Energy Rev 2019;116:109420. https://doi.org/10.1016/j.rser.2019.109420.

[22] Bao Z, Niu Z, Jiao K. Gas distribution and droplet removal of metal foam flow field for proton exchange membrane fuel cells. Appl Energy 2020;280:116011. https://doi.org/10.1016/j.apenergy.2020.116011.

[23] Yang X-G, Ye Q, Cheng P. Matching of water and temperature fields in proton exchange membrane fuel cells with non-uniform distributions. Int J Hydrogen Energy 2011;36:12524–37. https://doi.org/10.1016/j.ijhydene.2011.07.014.

[24] Fishman Z, Bazylak A. Heterogeneous Through-Plane Porosity Distributions for Treated PEMFC GDLs I. PTFE Effect. J Electrochem Soc 2011;158:B841. https://doi.org/10.1149/1.3594578.

[25] Kim S-G, Kim M-J, Sohn Y-J. Segmented cell approach for studying uniformity of current distribution in polymer electrolyte fuel cell operation. Int J Hydrogen Energy 2015;40:11676–85. https://doi.org/10.1016/j.ijhydene.2015.05.055.

[26] Zhang Q, Lin R, Técher L, Cui X. Experimental study of variable operating parameters effects on overall PEMFC performance and spatial performance distribution. Energy 2016;115:550–60. https://doi.org/10.1016/j.energy.2016.08.086.

[27] Meyer Q, Ronaszegi K, Robinson JBB, Noorkami M, Curnick O, Ashton S, et al. Combined current and temperature mapping in an air-cooled, open-cathode polymer electrolyte fuel cell under steady-state and dynamic conditions. J Power Sources 2015;297:315–22. https://doi.org/10.1016/j.jpowsour.2015.07.069.

[28] Heidary H, Kermani MJ, Dabir B. Influences of bipolar plate channel blockages on PEM fuel cell performances. Energy Convers Manag 2016;124:51–60. https://doi.org/10.1016/j.enconman.2016.06.043.

[29] Xing L, Du S, Chen R, Mamlouk M, Scott K. Anode partial flooding modelling of proton exchange membrane fuel cells: Model development and validation. Energy 2016;96:80–95. https://doi.org/10.1016/j.energy.2015.12.048.

[30] Park YH, Caton JA. Development of a PEM stack and performance analysis including the effects of water content in the membrane and cooling method. J Power Sources 2008;179:584–91. https://doi.org/10.1016/j.jpowsour.2008.01.050.

[31] Xing L, Cai Q, Xu C, Liu C, Scott K, Yan Y. Numerical study of the effect of relative humidity and stoichiometric flow ratio on PEM (proton exchange membrane) fuel cell performance with various channel lengths: An anode partial flooding modelling. Energy 2016;106:631–45. https://doi.org/10.1016/j.energy.2016.03.105.

[32] Candusso D, De Bernardinis A, Péra MC, Harel F, François X, Hissel D, et al. Fuel cell operation under degraded working modes and study of diode by-pass circuit dedicated to multi-stack association. Energy Convers Manag 2008;49:880–95. https://doi.org/10.1016/j.enconman.2007.10.007.

[33] Li X, Sabir I. Review of bipolar plates in PEM fuel cells: Flow-field designs. Int J Hydrogen Energy 2005;30:359–71. https://doi.org/10.1016/j.ijhydene.2004.09.019.

[34] Sajid Hossain M, Shabani B. Metal foams application to enhance cooling of open cathode polymer electrolyte membrane fuel cells. J Power Sources 2015;295:275–91. https://doi.org/10.1016/j.jpowsour.2015.07.022.

[35] Chen X, Chen Y, Liu Q, Xu J, Liu Q, Li W, et al. Performance study on a stepped flow field design for bipolar plate in PEMFC. Energy Reports 2021;7:336–47. https://doi.org/10.1016/j.egyr.2021.01.003.

[36] Bethapudi VS, Hack J, Hinds G, Shearing PR, Brett DJL, Coppens MO. Electro-thermal mapping of polymer electrolyte membrane fuel cells with a fractal flow-field. Energy Convers Manag 2021;250:114924. https://doi.org/10.1016/j.enconman.2021.114924.

[37] Trogadas P, Cho JIS, Neville TP, Marquis J, Wu B, Brett DJL, et al. A lung-inspired approach to scalable and robust fuel cell design. Energy Environ Sci 2018;11:136–43. https://doi.org/10.1039/c7ee02161e.

[38] Badduri SR, Srinivasulu GN, Rao SS. Influence of bio-inspired flow channel designs on the performance of a PEM fuel cell. Chinese J Chem Eng 2020;28:824–31. https://doi.org/10.1016/j.cjche.2019.07.010.

[39] Fontana É, Mancusi E, da Silva A, Mariani VC, Ulson de Souza AA, Ulson de Souza SMAG. Study of the effects of flow channel with non-uniform cross-sectional area on PEMFC species and heat transfer. Int J Heat Mass Transf 2011;54:4462–72. https://doi.org/10.1016/j.ijheatmasstransfer.2011.06.037.

[40] Akitomo F, Sasabe T, Yoshida T, Naito H, Kawamura K, Hirai S. Investigation of effects of high temperature and pressure on a polymer electrolyte fuel cell with polarization analysis and X-ray imaging of liquid water. J Power Sources 2019;431:205–9. https://doi.org/10.1016/j.jpowsour.2019.04.115.

[41] Rasha L, Cho JIS, Millichamp J, Neville TP, Shearing PR, Brett DJL. Effect of reactant gas flow orientation on the current and temperature distribution in self-heating polymer electrolyte fuel cells. Int J Hydrogen Energy 2021;46:7502–14. https://doi.org/10.1016/j.ijhydene.2020.11.223.

[42] Lochner T, Kluge RM, Fichtner J, El-Sayed HA, Garlyyev B, Bandarenka AS. Temperature Effects in Polymer Electrolyte Membrane Fuel Cells. ChemElectroChem 2020;7:3545–68. https://doi.org/10.1002/celc.202000588.

[43] Cheddie D, Munroe N. Parametric model of an intermediate temperature PEMFC. J Power Sources 2006;156:414–23. https://doi.org/10.1016/j.jpowsour.2005.06.010.

[44] Shao Y, Yin G, Wang Z, Gao Y. Proton exchange membrane fuel cell from low temperature to high temperature: Material challenges. J Power Sources 2007;167:235–42. https://doi.org/10.1016/j.jpowsour.2007.02.065.

[45] Salva JA, Iranzo A, Rosa F, Tapia E, Lopez E, Isorna F. Optimization of a PEM fuel cell operating conditions: Obtaining the maximum performance polarization curve. Int J Hydrogen Energy 2016;41:19713–23. https://doi.org/10.1016/j.ijhydene.2016.03.136.

[46] Wen D, Yin L, Piao Z, Lu C, Li G, Leng Q. Performance investigation of proton exchange membrane fuel cell with intersectant flow field. Int J Heat Mass Transf 2018;121:775–87. https://doi.org/10.1016/j.ijheatmasstransfer.2018.01.053.

[47] Mohsin M, Raza R, Mohsin-ul-Mulk M, Yousaf A, Hacker V. Electrochemical characterization of polymer electrolyte membrane fuel cells and polarization curve analysis. Int J Hydrogen Energy 2020;45:24093–107. https://doi.org/10.1016/j.ijhydene.2019.08.246.

[48] Wang G, Yu Y, Liu H, Gong C, Wen S, Wang X, et al. Progress on design and development of polymer electrolyte membrane fuel cell systems for vehicle applications: A review. Fuel Process Technol 2018;179:203–28. https://doi.org/10.1016/j.fuproc.2018.06.013.

[49] Zhang X, Yang Y, Zhang X, Guo L, Liu H. Performance Degradation of Proton Exchange Membrane Fuel Cell Caused by an Accelerated Stress Test. Fuel Cells 2019;19:160–8. https://doi.org/10.1002/fuce.201800152.

[50] Daud WRW, Rosli RE, Majlan EH, Hamid SAA, Mohamed R, Husaini T. PEM fuel cell system control: A review. Renew Energy 2017;113:620–38. https://doi.org/10.1016/j.renene.2017.06.027.

[51] Rojas JD, Kunusch C, Ocampo-Martinez C, Puig V. Control-Oriented Thermal Modeling Methodology for Water-Cooled PEM Fuel-Cell-Based Systems. IEEE Trans Ind Electron 2015;62:5146–54. https://doi.org/10.1109/TIE.2015.2405332.

[52] Yan C, Chen J, Liu H, Lu H. Model-Based Fault Tolerant Control for the Thermal Management of PEMFC Systems. IEEE Trans Ind Electron 2020;67:2875–84. https://doi.org/10.1109/TIE.2019.2912772.

[53] S++ Simulation Services n.d. http://www.splusplus.com/en/news.html (accessed May 13, 2021).

[54] Ou M, Zhang R, Shao Z, Li B, Yang D, Ming P, et al. A novel approach based on semi-empirical model for degradation prediction of fuel cells. J Power Sources 2021;488:229435. https://doi.org/10.1016/j.jpowsour.2020.229435.

[55] Cho J, Ko J, Park S. Comprehensive Analysis of Critical Factors Determining Limiting Current of PEMFC: O2 and H+ Transport Resistance without Cathode Humidification. J Electrochem Soc 2020;167:084511. https://doi.org/10.1149/1945-7111/ab8d71.